ISSN 1618-2642, Volume 397, Number 6

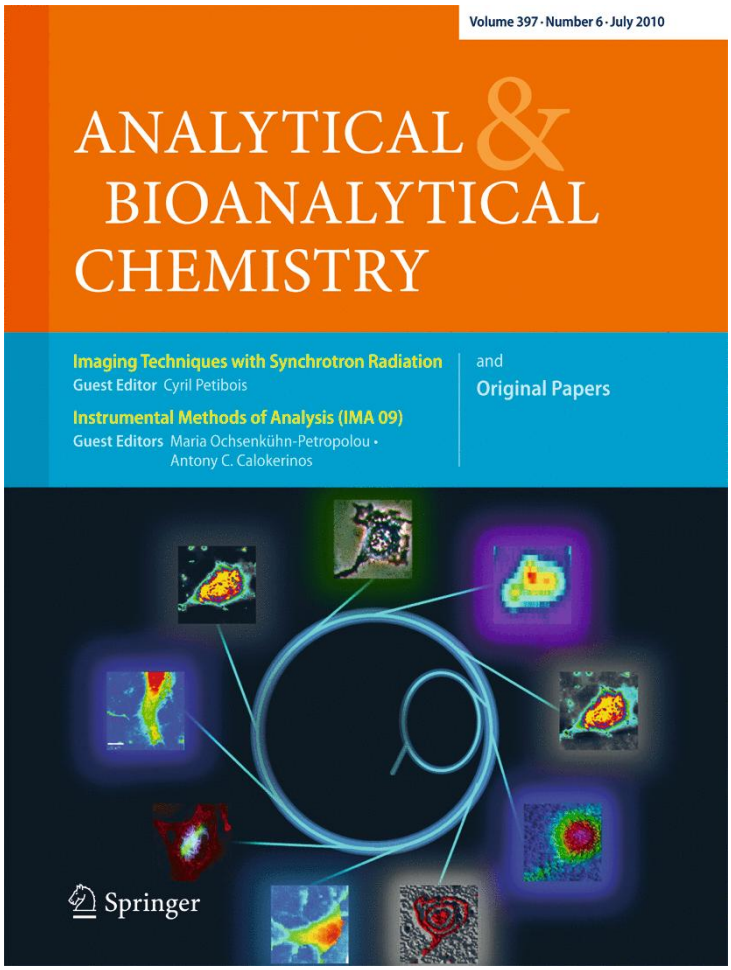

Anal Bioanal Chem (2010) 397:2131–2136
DOI 10.1007/s00216-010-3649-0

ORIGINAL PAPER

X-ray diffraction microtomography (XRD-CT), a novel tool for non-invasive mapping of phase development in cement materials

G. Artioli · T. Cerulli · G. Cruciani · M. C. Dalconi · G. Ferrari · M. Parisatto · A. Rack · R. Tucoulou

Received: 9 January 2010 / Revised: 8 March 2010 / Accepted: 9 March 2010 / Published online: 1 April 2010

Abstract A recently developed synchrotron-based imaging technique, X-ray diffraction microtomography (XRD-CT), has been applied here for the first time to a complex system, the hydrating Portland cement paste, in order to monitor the evolution of microstructure and phase formation with a 3D non-invasive imaging approach. The ettringite-XRD-peak-based image reconstructions, combined with transmission microtomography (X-μCT) images, allowed to assess the ubiquitous distribution of this phase, which appears early in the hydration process and showed its preferential concentration in the relatively less compact regions of the paste. The comparison of greyscale histograms for cement pastes after 9 and 58 h from hydration showed an increase of ettringite content with age, in agreement with the quantitative Rietveld analysis of the sum patterns. By renormalizing the greyscale histograms to the relative weight fraction, as obtained from Rietveld refinements, a new technique which allows estimation of phase contents with spatial resolution has been developed. The results achievable by combining XRD-CT, X-μCT and Rietveld appear very promising to provide experimental snapshots of the cement hydration process to be compared with results obtained from computer simulations.

Keywords Powder diffraction · Synchrotron · Microtomography · Imaging · Portland cements · Rietveld

G. Cruciani (✉)
Dipartimento di Scienze della Terra, Università di Ferrara,
44100 Ferrara, Italy
e-mail: cru@unife.it

G. Artioli · M. C. Dalconi · M. Parisatto
Dipartimento di Geoscienze, Università di Padova,
35122 Padua, Italy

T. Cerulli · G. Ferrari
Analytical Laboratory, MAPEI S.p.A.,
20158 Milan, Italy

A. Rack · R. Tucoulou
European Synchrotron Radiation Facility,
38043 Grenoble, France

Introduction

The property of cementitious materials to develop mechanical strength when mixed with water results from a complex set of chemical, physical and microstructural processes taking place during hydration. Although the overall chemical reactions and physical changes occurring during hydration are known, we have limited knowledge of the mechanisms involved in the microstructural development of the hydrating paste. A major issue concerns the location where the hydration products preferentially develop in relation to the reacting Portland clinker phases (C3S, C2S, C3A and C4AF; cement chemistry notation: C = CaO, S = SiO_2, A = Al_2O_3, F = Fe_2O_3 and H = H_2O) and their relationships with evolution of the paste physical properties.

Backscattered electron (BSE) imaging has been widely used to examine the microstructure of hydrated cementitious materials [1–4]. BSE imaging provides compositional contrast (mean atomic number) allowing individual phases to be differentiated and quantified using image analysis. However, the mean backscatter coefficient for several hydration products (C–S–H, ettringite, AFm phases) are too close to be individually distinguished and the quantification of microstructural characteristics is restricted to unreacted cement phases, portlandite (CH) and porosity.

Reliable BSE imaging requires careful preparation of flat, polished surfaces of dried specimens. Only two-dimensional sections of a three-dimensional microstructure can be observed in a destructive manner.

X-ray microtomography (X-μCT) has recently been applied on cement materials for characterising their 3D microstructural features [5–10]. This technique offers the great advantage of imaging the internal structure of the object in an almost non-invasive manner. Investigating materials without perturbing the micro-structures is fundamental when the physical properties of the materials are dependent on the evolution of the intimate organisation of the structure. However, X-μCT clearly shows features having high-density contrast, such as voids and fractures within the solid material, though different crystalline or amorphous phases with similar density and composition are hardly distinguished.

A 3D non-invasive imaging technique (approximately micrometre spatial resolution) with added chemical and crystal phase selectivity has been recently proposed combining absorption-, fluorescence- and diffraction-microtomography [11]. In particular, XRD-CT (X-ray diffraction microtomography) represents a powerful and very promising method combining the principles of X-ray powder diffraction and microtomography to map the spatial distribution of a selected crystalline or amorphous phase inside a sample with a non-invasive approach. The functioning of combined X-ray fluorescence and diffraction microtomography setup was also tested and illustrated by De Nolf et al. [12].

This paper reports the first application of XRD-CT to cementitious materials combined with X-μCT. The aims of the present study were to assess the feasibility of scanning tomography with a powder diffraction-based contrast on complex heterogeneous systems such as mortar and cement samples. The study was also motivated by the need of experimental data on the hydration products distribution to be compared with simulated microstructure models as obtained by 3D computer modelling of hydrating cement [13, 14].

Experimental

Materials

Ordinary Portland cement and mortar samples were used in this study. The cement sample was prepared by mixing a CEM I 52.5 R powder with deionized water according to a water to cement ratio (*w*/*c*) of 0.5. The paste was mixed by hand for 30 s and inserted in a 500-μm diameter glass capillary (borosilicate glass capillary, wall thickness 10 μm). A small portion of the tube capillary was filled by gently sliding the paste inside and then sealed with plasticine at both ends. The syringe injection method was avoided because it can induce bleeding effects (water is squeezed away).

For the preparation of the mortar sample, a very fine sand composed of quartz and feldspar grains was added. A CEN standard sand (Société Nouvelle du Littoral) conforming to the EN-196-1 norm ("Methods of testing cement; determination of strength") was sieved in order to separate the granulometric fraction between 80 and 100 μm. This fraction was then passed through an isodynamic magnetic separator in order to separate quartz and feldspar grains from all the other minerals of the sand. The mortar sample was then prepared by mixing the CEM I 52.5 R powder, the separated sand and deionized water, according to a 2:1:1 mass proportion.

Microtomography measurements

X-ray absorption and X-ray diffraction tomographic scans were performed at the European Synchrotron Radiation Facility (ESRF, Grenoble, France) at the ID22 beamline [15]. The experimental setup of the beamline did not allow simultaneous measuring of X-μCT and XRD-CT data on the same sample, so it was necessary to move the goniometer head with the sample capillary on different sample stages for the two kinds of measurements. Nevertheless, it was possible to compare X-μCT and XRD-CT images of approximately the same capillary cross-sections.

X-ray microtomography

For each sample, several high resolution tomographies were performed at different times of the hydration process (from 1 to 72 h) in order to monitor the microstructural evolution of the reacting material. The electron beam current in the storage ring was about 200 mA, while the energy of the incident X-ray beam was kept fixed at 14 keV using a double-crystal monochromator. For each complete 180° scan, 1,800 projections with an angular step of 0.1° were acquired using a FReLoN CCD camera [16] working with a 20× optical magnification; the resulting pixel resolution was ~0.7 μm. Acquisition times ranged from 0.650 to 0.875 s according to the composition and thickness of the sample and to the amount of beam flux decay with time. These experimental conditions represented the best compromise between acquisition times (approximately 40 min/scan) and signal to noise ratio (i.e. image quality) and ensured negligible heating and drying of cement during the data collection. The reconstruction of the tomographic cross-sectional slices was carried out using the Filtered Back Projection algorithm [17] via the ESRF software package PyHST [18].

X-ray diffraction microtomography

The experimental setup for XRD-CT included a monochromatic (E=18 keV) and collimated 2×4 μm^2 beam, a FReLoN fibre-optic taper CCD for fast data acquisition, and a sample stage which allowed precise translational and rotational movements. XRD-CT is based on recording diffraction data while translating (along y, perpendicular to the incident beam direction) and rotating (ω, around vertical z axis) the sample irradiated by the pencil beam. 2D diffraction patterns were recorded using 4-μm steps in the horizontal scan (along y), and scans were taken over 180° rotation (ω) with steps of 3°. Thus, for sampling a 500 μm capillary sample, 108×60 diffraction measurements were acquired, each measurement requiring an acquisition time of 0.8 s, for a total measuring time of 8 h. Azimuthal integration of the 2D diffraction patterns allowed to obtain a series of 1D diffraction profiles where regions of interest (ROIs), corresponding to different scattering contributions, were selected in order to extract sinograms Sp(y,ω) relative to specific phases (Fig. 1). Tomographic reconstruction provided the variation of the intensity of any diffraction ROI as a function of x, y, z, thus obtaining axial slices of the corresponding phases. The XRDUA software package (v2.0.0.4) [19] was used for the entire process of calibration and correction of 2D-diffraction frames, azimuthal integration, sinograms extraction and tomographic reconstruction. Diffraction frames were corrected for spatial distortion and dark current, sinograms were normalised for the incident beam intensity (which decays with time due to the finite lifetime of storage ring beam current), and the MLEM (maximum-likelihood expectation–maximisation) algorithm was used for tomographic reconstruction. The reconstructed images (tomograms) have a final voxel size

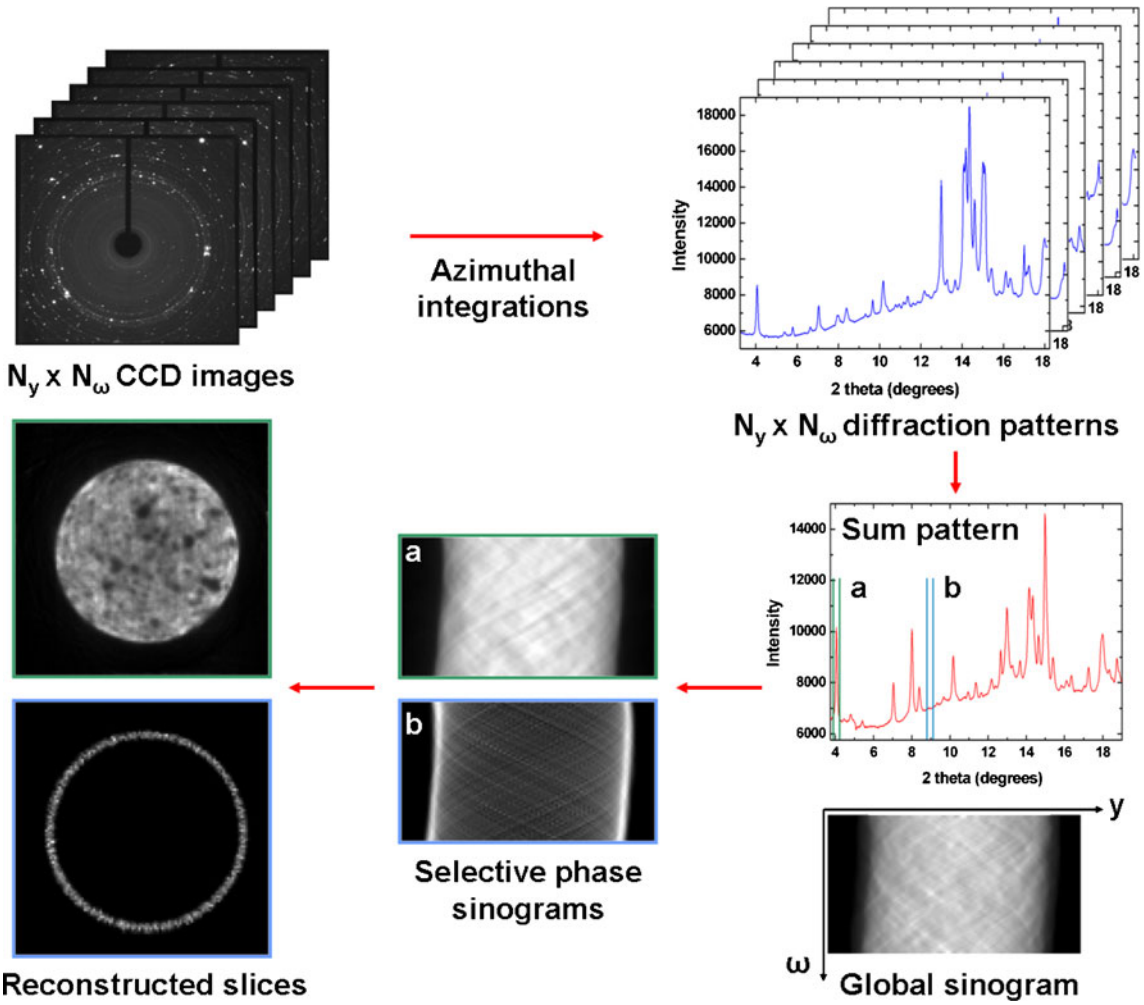

Fig. 1 Reconstruction scheme of the XRD-CT analysis: for every translation (y) and rotation (ω) of the sample, a 2D diffraction pattern is collected, thus obtaining a set of azimuthal integrated linear diffraction patterns. Regions of interest corresponding to a particular 2θ range (e.g., a single peak) are selected on the linear diffraction patterns to build up sinograms, representing the variations of the diffracted intensity as a function of y and ω. Sinograms are then used to reconstruct cross-sections mapping the spatial distribution of selected phases of interest (sinogram a refers to ettringite while sinogram b to the glass capillary)

of 4×4×2 μm^3 corresponding to the isotropic (x, y) sampling of the reconstructed slice and to the slice thickness equal to the vertical beam dimension.

XRD-CT data were collected on the mortar sample at ~12 h from hydration. The mortar sample was chosen in order to verify the XRD-CT feasibility on a highly heterogeneous system both in composition and grain size. The cement sample was scanned at 9 and 58 h from hydration in order to test the XRD-CT capabilities in monitoring the evolution of cement hydration over time.

Results and discussion

The XRD-tomogram based on the 001 peak intensity of the newly formed ettringite phase, $Ca_6Al_2(SO_4)_3(OH)_{12}{\cdot}26H_2O$, is shown in Fig. 2. Pixels with different grey values indicate different amount of ettringite crystals inside the volume sampled by the beam (4×4×2 μm^3). The sub-micrometre sized ettringite crystals were one order of magnitude smaller than the probe size. The sampled volume thus contained a sufficiently large number of ettringite crystals to give optimal powder diffracted intensities, and the corresponding tomogram was easily reconstructed. Large well-diffracting crystals of quartz and clinker phases behaved as "single-crystals" and tomogram reconstruction for these phases was affected by severe artefacts hampering their mapping. The black pixel areas in ettringite tomogram of the mortar sample (Fig. 2a) correspond to quartz grains, macro voids and unreacted clinker grains. These coarse features are in agreement with the microstructural characteristics visible in the higher resolution X-μCT tomogram of approximately the same mortar slice (Fig. 2b). The good correspondence between the X-μCT and XRD-CT features confirms the reliability of the tomogram reconstruction based on the 001 ettringite peak intensity.

Unperturbed phase distribution of ettringite was also obtained for cement samples (Fig. 3). Changes in ettringite distribution as a function of hydration were monitored by comparing the grey values histograms of the same sample measured at different times from hydration (8 and 58 h, Fig. 3c). As the age of the cement sample increases, the large peak in the histogram shifts to higher grey values indicating an increase of ettringite volume fraction per pixel. Ettringite weight fractions inside the sampled slices were estimated by means of Rietveld refinements on the averaged diffraction patterns, and the obtained results (14 and 22 wt.% at 9 and 58 h, respectively) confirmed the increase of ettringite as detected by XRD-CT. Because it was not possible to quantify the amorphous content (e.g., C–S–H), the obtained weight fractions are not absolute values and were used just to compare the phase evolution in the cement sample with hydration.

The evolution of the microstructure during hydration was also monitored by the greyscale histograms determined over a volume of interest (400×400×250 voxels, voxel size = 0.7 μm) extracted from the X-μCT tomograms (Fig. 3d). The peak with decreasing height as the age of the sample increases corresponds to unreacted cement (UC), whereas the peak with increasing area indicates the increasing population of hydration products (HP). Porosity (P) generates the peak shoulder visible in the lower range of grey values and overlaps with the grey level of hydration products.

The image in Fig. 3a also shows that ettringite is ubiquitously distributed inside the capillary sample with slightly higher concentration in areas close to the capillary walls. A non-homogeneous distribution of the paste is also visible in the X-μCT image (Fig. 3b), where it can be observed that the compactness of the paste increases from the capillary walls towards the centre. This preferential formation of ettringite in less compact areas of the paste can be interpreted as due either to the favoured circulation of sulphate -rich pore solution near the capillary walls or to the difficulties in achieving homogeneous filling of the capillary.

The histograms in Fig. 3c can be re-normalised in such a way that the curve integrals (greyscale times voxels) are set equal to the relative weight fraction of ettringite as obtained by Rietveld. The obtained plots of wt.% fraction vs.

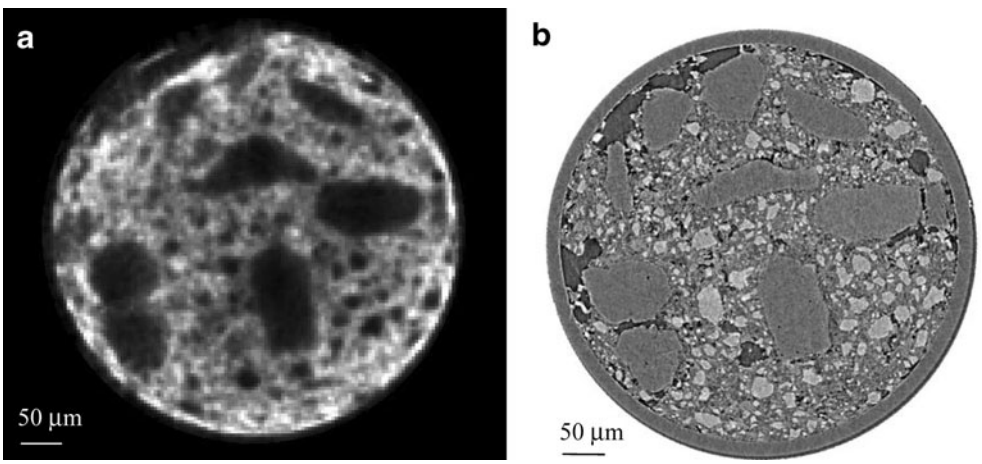

Fig. 2 **a** XRD-tomogram based on the 001 peak intensity of ettringite phase in the mortar sample. **b** X-μCT tomogram of the mortar sample. Reconstructed images **a** and **b** correspond approximately to the same cross-section of the mortar sample

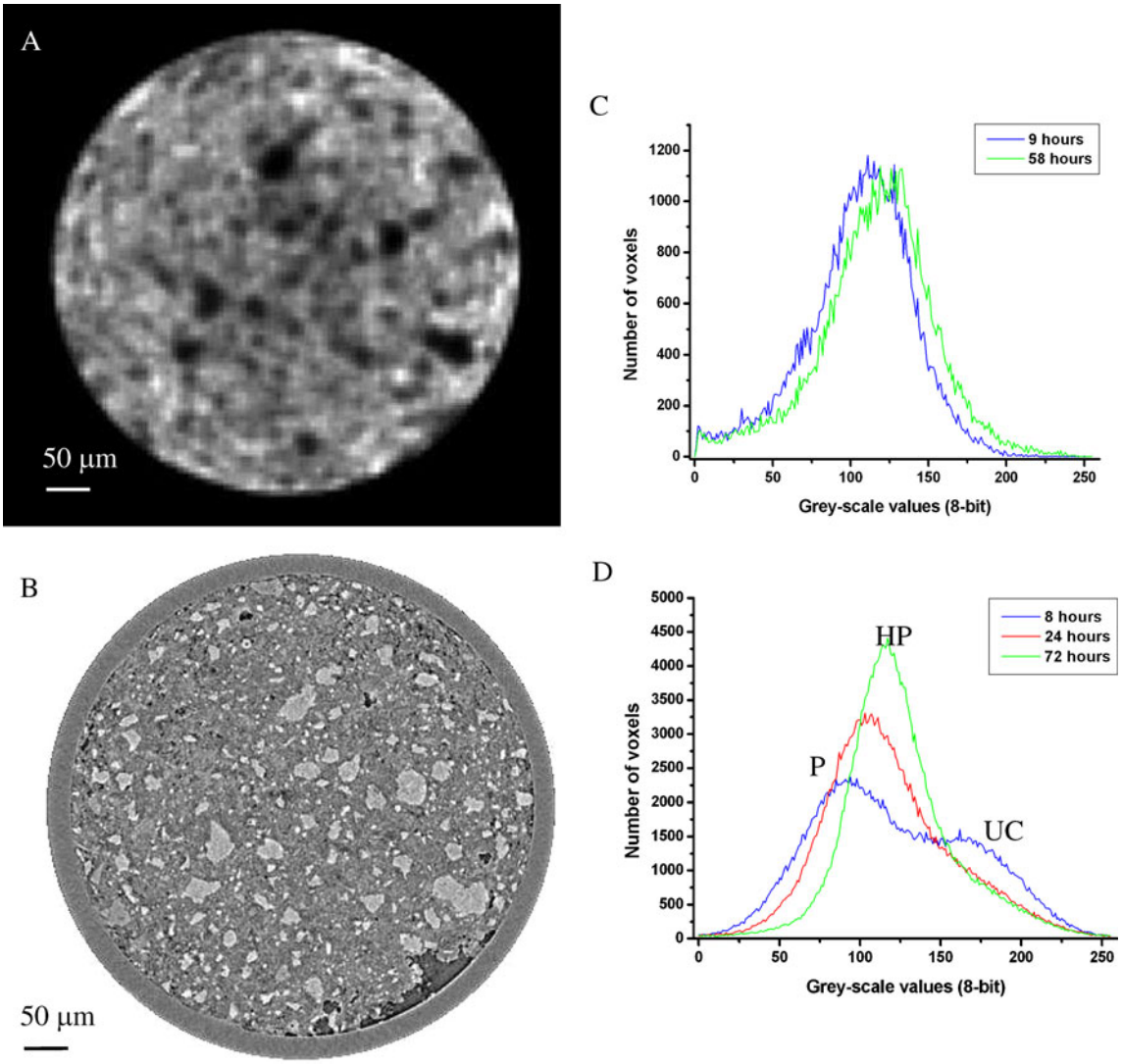

Fig. 3 **a** XRD-tomogram based on the 001 peak intensity of ettringite phase in the cement sample at 58 h from hydration. **b** X-µCT tomogram of the same cross-section of the cement sample at 48 h from hydration. **c** Change in grey value histograms relative to ettringite tomograms of the cement sample at 9 and 58 h from hydration. **d** Histograms of grey values (proportional to linear attenuation coefficient) for hydrated cement after 8, 24 and 72 h. The histograms were determined over the 3D X-µCT tomograms (*UC* unreacted cement, *HP* hydration products; *P* porosity)

greyscale provide an estimation of the local content of ettringite associated to any given greyscale value down to a lower limit of about 0.1 wt.%.

Conclusions

On the basis of the results of these test measurements, it can be concluded that XRD-CT can be successfully applied for the three-dimensional investigation of cement materials in a totally non-invasive way. The main advantage is the access to the real distribution of selected crystalline or amorphous phases. This method allowed to map the ettringite distribution in mortar and cement samples and its evolution with hydration.

The main problems encountered concern artefacts in tomographic reconstruction for phases with crystal sizes comparable to the dimension of the incident beam. Effective correction strategies need to be developed. Other drawbacks are the limited spatial resolution (4 µm in the present study) compared to the X-µCT, and the long acquisition time for a complete XRD tomographic scan over a 500 µm diameter sample. The long acquisition time does not match the time resolution required for studying paste evolution during the early stages of hydration. This limitation can partially be overcome by reducing the size of the measured volume thus reducing the total acquisition time. As a general conclusion, we can say that the limits of applicability of the technique concern the dimensions of

crystalline objects that can be mapped in relation to the obtainable spatial resolution. The main constraint in obtaining phase mapping is to have crystals which are one order of magnitude smaller than the X-ray beam size. Increasing the beam size, crystalline materials with larger crystals can be mapped but at the expense of spatial resolution.

Despite the present limitations, XRD-CT is a powerful and very promising method to map the distribution of phases, irrespective on their crystalline nature, with a 3D non-invasive approach.

This technique can offer 3D imaging experimental data to compare with 3D computer simulation of cement hydration and microstructure changes.

The combined XRD-tomography-Rietveld method developed here for the first time is capable to provide spatially resolved estimation of phase fractions allowing semi-quantitative mass balance calculations to be added in the microstructure modelling. The accuracy and precision of these calculations will be mainly dependent on the amount of amorphous phase(s) developed during the cement hydration process. These are comparable to accuracy and precision of Rietveld quantitative phase analyses typically reported in the literature for cementitious materials (e.g., [20]).

Acknowledgements The European Synchrotron Radiation Facility is acknowledged for provision of synchrotron radiation beamtime (exp MA-648). We sincerely thank Jakub Jaroszewicz for his kind help in getting us started with XRDUA. The experiment has been performed in the frame of the MAPEI-UNIPD research agreement.

References

1. Scrivener KL, Pratt PL (1984) Proc 6th Int Conf Cem Microscopy, Albuquerque, New Mexico, p 145
2. Wang Y, Diamond S (1995) Mater Res Soc Symp Proc 370:23
3. Scrivener KL (2004) Cem Concr Compos 26:935–945
4. Wong HS, Head MK, Buenfeld NR (2006) Cem Concr Res 36:1083–1090
5. Garboczi EJ (2002) Cem Concr Res 32:1621–1638
6. Chotard TJ, Boncoeur-Martel MP, Smith A, Dupuy JP, Gault C (2003) Cem Concr Res 25:145–152
7. Garci Juenger MC (2004) Concr Int 26:38–41
8. Helfen L, Dehn F, Mikulik P, Baumbach T (2005) Adv Cem Res 17:103–111
9. Gallucci E, Scrivener K, Groso A (2007) Cem Concr Res 37:360–368
10. Diamond S, Landis E (2007) Mater Struct 40:989–993
11. Bleuet P, Welcomme E, Dooryhée E, Susini J, Hodeau J-L, Walter P (2008) Nat Matters 7:468–472
12. De Nolf W, Janssens K (2009) Surf Interface Anal (www.interscience.wiley.com) doi:10.1002/sia.3125
13. Bentz DP (1999) Mater Struct 32:187–195
14. Bishnoi S, Scrivener KL (2008) Cem Concr Res 39:266–274
15. Weitkamp T, Raven C, Snigirev A (1999) Proc of SPIE, Bonse U editor, 3722:311–317
16. Labiche JC, Mathon O, Pascarelli S, Newton MA, Guilera Ferre G, Curfs C, Vaughan G, Homs A (2007) Rev Sci Instrum 78:091301
17. Kak AC, Slaney M (1988) Principles of computerized tomographic imaging. IEEE, New York, 1988
18. PyHST (High Speed Tomographic Reconstruction) by Mirone A, Wilcke R, Hammersley A, Ferrero C (2009) http://www.esrf.eu/UsersAndScience/Experiments/TBS/SciSoft/
19. XRDUA Software Package by Wout De Nolf, http://xrdua.ua.ac.be
20. Merlini M, Artioli G, Meneghini C, Cerulli T, Bravo A, Cella F (2007) Powder Diffract 22:201–208